The Journal of Experimental Biology 214, 2381-2389

doi:10.1242/jeb.056671

RESEARCH ARTICLE

Building a robotic link between muscle dynamics and hydrodynamics

Christopher T. Richards
The Rowland Institute at Harvard, Harvard University, Cambridge, MA 02142, USA
richards@fas.harvard.edu

Accepted 14 April 2011

SUMMARY

This study used a novel feedback approach to control a robotic foot using force and length signals transmitted from an isolated *Xenopus laevis* frog muscle. The foot's environment (inertial *versus* hydrodynamic), gearing (outlever/inlever) and size were changed to alter the muscle's load. Upon nerve stimulation (250 Hz, 80 ms train duration), variation in loading generated a range of muscle stress (19.8±5.3 to 66.0±22.5 kPa), work (1.89±0.67 to 6.87±2.96 J kg^{-1} muscle) and power (12.4±7.5 to 64.8±28.3 W kg^{-1} muscle; mean ± s.d., *N*=6 frogs). Inertial *versus* hydrodynamic loading dramatically shifted contractile dynamics. With the foot in water, the muscle generated ~30% higher force, yet shortened slower, producing lower power than inertial loading. Power increased in air from 22.6±5.8 to 63.6±27.2 W kg^{-1} muscle in response to doubling the gear ratio, but did not increase in water. Surprisingly, altering foot size diminished muscle performance in water, causing power to drop significantly from 41.6±11.1 to 25.1±8.0 W kg^{-1} muscle as foot area was doubled. Thus, morphological modifications influenced muscle dynamics independently of neural control; however, changes in loading environment and gearing affected contractile output more strongly than changes in foot size. Confirming recent theory, these findings demonstrate how muscle contractile output can be modulated solely by altering the mechanical environment.

Key words: muscle power, biorobotics, gearing.

INTRODUCTION

Physiologists have established the importance of the nervous system for controlling locomotion, relying on electromyography (EMG) to probe muscle function during running, flying and swimming (e.g. Freadman, 1979; Mann and Hagy, 1980; Dial et al., 1987). For example, EMG magnitude increases with swimming speed in fish (e.g. Rome et al., 1984), suggesting that the nervous system increases the motor neuron firing rate (e.g. Tanji and Kato, 1973) and activates additional muscle fibers (Roberts et al., 1997) to increase work output. *In vivo* force measurements further enrich our understanding of neural input *versus* muscle mechanical output. In certain conditions, EMG signals predict changes in muscle work (Roberts et al., 1997; Daley and Biewener, 2003; Hedrick et al., 2003; Richards and Biewener, 2007). However, when running guinea fowl encounter unexpected drops in floor height, muscle-tendon force instantaneously decreases, demonstrating how muscle dynamics are governed not only by neural activation, but also by the mechanical environment (Daley et al., 2009). These insights are crucial for understanding locomotion. Yet, *in vivo* approaches cannot entirely distinguish muscle–environment interactions from neural control. In eels, for example, dramatic differences in muscle function on land *versus* water are likely due to activation patterns co-varying with muscle–environment interactions (Gillis, 2000). Current physiological tools cannot isolate muscle–environment effects, and thus cannot effectively link neural control with muscle mechanical output. To bridge this gap, the present study introduces a novel biorobotic tool that measures the force–length dynamics of an isolated *Xenopus laevis* muscle as it drives a robotic limb in water.

Complementing *in vivo* studies, additional understanding of muscle dynamics comes from the *in vitro* 'work loop' approach (Machin and Pringle, 1960; Josephson, 1985). Such experiments measure force emerging from force–velocity (F–V) (Hill, 1938), force–length (F–L) (Gordon et al., 1966) and work history (Josephson, 1999) properties, which dictate force output at a given length and velocity. Further, the F–V curve predicts maximum power at shortening speeds of approximately one-third maximum shortening velocity (V_{max}). For instance, fast length oscillations (near V_{max}) may produce low power typical of a light load (e.g. a leg swinging through air), whereas slower length oscillations (~1/3 V_{max}) reproduce higher force and power required to move a resistive load (e.g. a leg in water). Thus, altering the shape or magnitude of the input length pattern implicitly changes the loading environment, thus influencing muscle mechanical output.

In cyclic swimming and flying, a muscle's loading environment is adequately simulated by simple length change patterns of work loop preparations (e.g. Altringham and Johnston, 1990; Askew and Marsh, 1997). However, because of the complexity of limb motion during unsteady swimming (e.g. Gal and Blake, 1988), traditional work loops might misrepresent *in vivo* muscle loads, especially when probing muscle function beyond the *in vivo* range. Faced with this complexity, how do we explore muscle function coupled to realistic fluid-dynamic loads?

Numerical models address muscle–fluid interactions by simultaneously calculating muscle force and fluid reaction force (Daniel and Meyhofer, 1989; Daniel, 1995; Aerts and Nauwelaerts, 2009). For instance, swimming models reproduce realistic swimming motions from muscle–fluid interactions (Ekeberg, 1993; Ijspeert et al., 2005; Ijspeert et al., 2007; Tytell et al., 2010), but fail when hydrodynamics are absent (Bowtell and Williams, 1991). Additionally, skeletal gearing (outlever to inlever ratio) further influences power transmission from muscle to the load. For example, how do changes in muscle moment arm length affect the muscle

power required to move a load? Do certain skeletal modifications suit a particular environment? Although numerical approaches help address these questions, models capturing the interesting parameters may be impossible to verify and too cumbersome for widespread use.

Here, I introduce a novel tool to measure dynamic interactions between muscle and a hydrodynamic load. Similar to the work loop technique, the present study records dynamic force from an isolated muscle. However, instead of arbitrary length control, the muscle shortening pattern results from its instantaneous mechanical interaction with the robotic limb as it moves through water. I experimentally manipulated both the external anatomy (foot size) as well as the skeletal anatomy (gearing) to explore the muscle function of a frog limb in the presence or absence of a fluid dynamic load. Three manipulations were expected to increase muscle force and power: (1) immersion in water (fluid loading) *versus* air (inertial loading), (2) increasing the limb's gearing by shortening the muscle moment arm (increasing rotation speed and propulsive force for a given muscle velocity) and (3) increasing fluid drag by increasing the foot size. For inertial loading, low gear and small foot size, the muscle is expected to produce low forces (thus low power). Upon manipulations 1–3, increased load from the environment is expected to require higher forces at reduced shortening velocities, thus increasing power. The plantaris longus (PL) muscle from the aquatic frog *Xenopus laevis* was used as a model for the present study. Findings presented here give new insights about the importance of skeletal and limb design on the muscle power requirements of swimming.

MATERIALS AND METHODS

Animals

Adult male *Xenopus laevis* (Daudin 1802) (25.0±7.2 g, mean ± s.d. body mass, N=6; Table 1) purchased from Xenopus Express, Inc. (Plant City, FL, USA) were housed in glass aquaria at the Rowland Institute and maintained at 20–22°C under a 12 h:12 h light:dark cycle. All experimental protocols used were approved by the Harvard University Institutional Animal Care and Use Committee.

In vitro muscle preparation

The PL muscle was selected because of its prominent propulsive role in the specialized swimmer *X. laevis* (Richards and Biewener, 2007) and for its parallel fiber architecture [unlike the pinnate architecture found in other species (e.g. Roberts and Marsh, 2003)]. Frogs were double pithed with a 21 gauge syringe needle. Prior to dissecting muscles from the leg, resting PL muscle length (L_{rest}) was measured by the following procedure. The hip, knee, ankle and tarsometatarsal joints were positioned at 90 deg angles approximating the midpoints of *in vivo* joint excursions (Ahn et al., 2003). L_{rest} (assumed to be the optimal length, L_{opt}) was measured as the longest portion of the muscle between the tendon and aponeurosis. All muscles surrounding the origin of the PL were removed, leaving the sciatic nerve intact. The femur was then cut roughly 0.5 cm from the knee. Using a 21 gauge syringe needle, a hole was bored through the knee. A size 3 metric multifilament nylon Braunamid™ suture was then thread from the hollow (cut) end of the femur bone through the hole made at the knee joint. This suture was later used to anchor the proximal end of the muscle to the muscle ergometer. To provide a distal anchor to the ergometer, another suture was tied between the PL tendon and the proximal tarsal bones near the ankle joint. The stiff connective tissue sheath around the tendon anchored the suture to the proximal tarsal bones. All remaining bone and musculature were removed, isolating the PL. Finally, the foot was cut off roughly 0.5 cm distal to the suture. Enough proximal tarsal bone was left to anchor the suture; however, excess bone was removed to minimize mass. To mount the muscle in the ergometer, the proximal suture was tied to a stiff metal pin embedded in Plexiglas®, immobilizing the muscle's proximal end. The distal suture was then tied through a small hole in the muscle lever connected to a 305C-LR servo motor (Aurora Scientific, Inc., Aurora, ON, Canada). During experimental trials, the muscle was bathed in 22°C (matching the temperature of the frog housing facility) oxygenated amphibian Ringer solution (Carolina Biological, Burlington, NC, USA).

Muscle–robotic feedback loop

A novel approach was used to allow a *X. laevis* PL muscle to control the motion of a rotating robotic foot. Two mechanical rigs were necessary. First, a robotic platform was built to rotate a robotic foot (to simulate rotation of a frog foot during swimming, Fig. 1A). The platform rested above a 20 gallon glass aquarium, allowing the foot to either be submerged (for hydrodynamic loading) or raised above the water surface (inertial loading). *Xenopus laevis* is an ideal model for biorobotics, in part because thrust is mainly produced by foot rotation (as opposed to rotation and translation) (Richards, 2010). Importantly, the present setup only mimics the initial kick of a *X. laevis* swimming sequence. In the first kick, the foot has been observed to rotate in still water while the limbs extend as the body advances forward. Foot rotation was powered by a 305C-LR servo motor (Aurora Scientific, Inc.) configured in force-control mode. Second, a 'work loop' ergometer was used for *in vitro* muscle measurements (Fig. 1B). Both the robotic limb and the ergometer were electronically linked by a computer-controlled feedback loop. Instead of controlling the position of the robotic fin, the force signal simultaneously measured from the contracting muscle was used as the control signal for the robot. Likewise, instead of arbitrarily controlling the position of the muscle, the muscle length signal came from the robotic foot's position. Therefore, a feedback loop allowed muscle force to control the robot's force against the water while foot displacement controlled muscle length. Both muscle position and robot torque were updated every 0.1 ms using a National Instruments cRIO-9074 field programmable gate array (FPGA) Real-Time Controller (Austin, TX, USA). In a typical trial at the first instant following muscle stimulation, the muscle produces force isometrically. Simultaneously, this force is applied to the robotic

Table 1. Morphology of *Xenopus laevis* used in the present study

Frog	Mass (g)	Plantaris longus muscle mass (g)	Muscle fascicle rest length (mm)	Muscle cross-sectional area (cm^2)
1	24.4	0.74	22.26	0.31
2	22.2	0.69	22.56	0.29
3	39.6	1.29	25.09	0.49
4	20.4	0.70	20.75	0.32
5	22.1	0.58	21.02	0.26
6	21.6	0.70	20.63	0.32

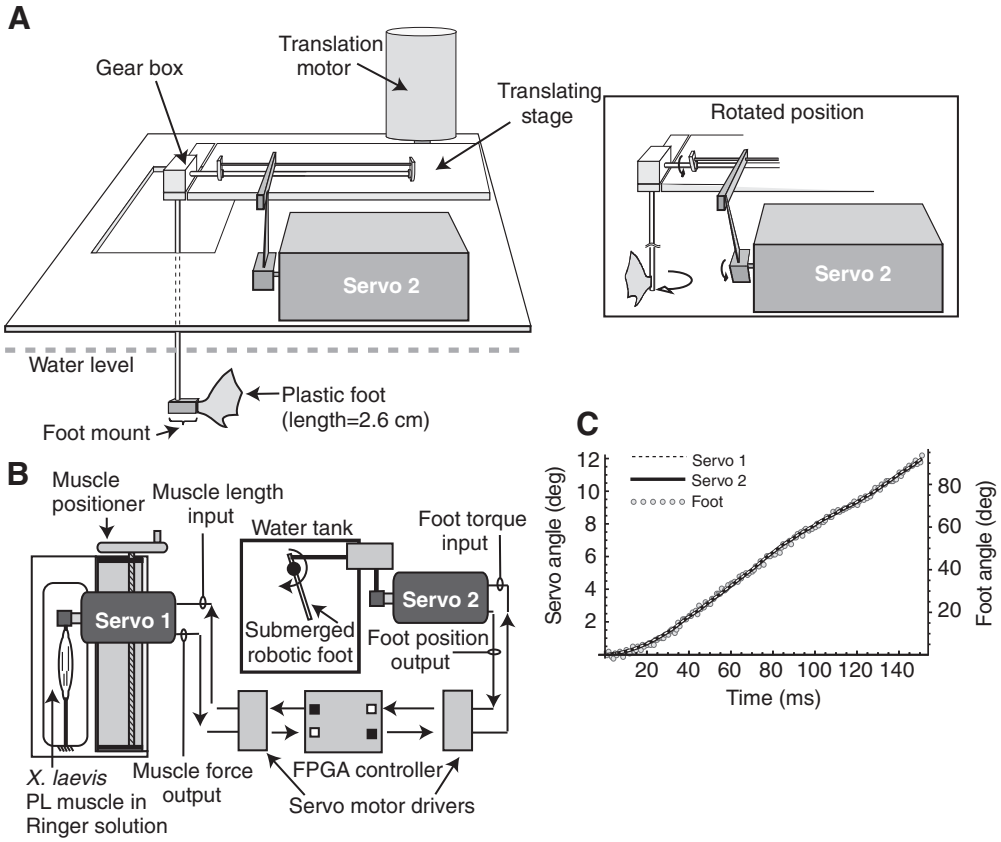

Fig. 1. (A) Servo 2 acts through a simple linkage to rotate a robotic foot. Separately, a large servo motor (not used in the present study) can translate the foot. (B) A muscle ergometer (Servo 1) measures muscle force in response to electrical stimulation from a suction electrode (not shown). At each instant in time, muscle force recorded by Servo 1 passes through a field programmable gate array (FPGA) controller as a command signal for Servo 2. Instantaneously, Servo 2 exerts force (recorded from the muscle) against the mechanical limb. Servo 2 then records the resulting robotic foot displacement signal, which returns through the FPGA module to command Servo 1. This forms a feedback loop enabling the muscle to shorten as if directly attached to the foot. (C) Testing the mechanical linkage by manually pulling the muscle lever of Servo 1 shows nearly identical displacement traces from Servos 1 and 2 and the robotic foot. Data traces were not processed.

foot, which displaces in the fluid. After 0.1 ms, the ergometer shortens the muscle to match the displacement of the robotic limb. Consequently, the muscle contracts as if pulling directly on the mechanical linkage driving foot rotation. Trace recordings of muscle stimulation, muscle force, muscle length and robot position were recorded at a sample rate of 4 kHz using a National Instruments USB-6289 A/D board.

Muscle stimulation

The PL muscle was stimulated *via* the sciatic nerve with a suction electrode. Stimulation pulses of 1 ms width were generated from the A/D board and amplified by an OPA549T op-amp (Texas Instruments, Dallas, TX, USA) powered by a Protek 3003B power supply (Protek Devices, Tempe, AZ, USA) to provide enough power to fully stimulate the muscle. Isometric twitch contractions were used to determine the maximal stimulation voltage. For all experimental trials, the muscle was stimulated with an 80 ms pulse train at supramaximal voltage at a spike frequency of 250 Hz (Fig. 2) based on *in vivo* EMG patterns previously observed in the PL muscle of *X. laevis* (Richards and Biewener, 2007). Voltage stimulation was generated from an amplified computer analog output signal. Each data point collected was from a single muscle contraction (a series of cyclic contractions could not be performed in this setup; see Discussion).

Mimicking frog anatomy in the bio-robot

The robotic foot was fabricated from 1.57 mm thick Plexiglas®. To mimic the shape of frog feet, a digital tracing of a *X. laevis* foot was used as a template to be cut by an Epilog Mini 35 W laser cutter (Epilog Laser, Golden, CO, USA) to sizes of 50, 100 and 150% of the length of actual *X. laevis* feet (areas=1.2, 4.7 and 10.6 cm^2).

Gear ratio was defined as outlever (OL)/inlever(IL). IL is the muscle moment arm, i.e. the perpendicular distance between the muscle's line of action and the joint center of rotation. OL was approximated to be the constant distance between the center of foot rotation and center of area of the robotic foot (see Discussion). Changes in gear ratio were performed electronically by manipulating the force and displacement constants with a gearing multiplier (GM) within the muscle–robot feedback loop software. For example, to double the gearing multiplier (GM=2), the angular displacement of the ergometer muscle lever was multiplied by two to give the displacement transmitted to the robot foot. Likewise, muscle force was divided by two to calculate the force transmitted to the robot foot. This is mechanically equivalent to changing the muscle's insertion such that small muscle length changes effect relatively larger angular displacements (but proportionally less force) at the foot. In addition to the software-controlled GM, a mechanical gearbox was used to sufficiently amplify the angular displacement of the servo motor, resulting in a muscle IL (≈muscle displacement/foot angular displacement) of 5.25 mm, which is within the approximate range measured for the *X. laevis* PL muscle. For *X. laevis*, IL distance remains constant over the range of joint excursion used during swimming (data not shown). Importantly, because OL distance was assumed constant, changes in GM are equivalent to changes in gear ratio. For the present study, GM=1 resulted in an IL length of 5.25 mm (gear ratio≈5). Doubling and quadrupling GM was achieved by dividing the virtual IL by 2 (IL=2.88 mm; gear ratio≈10) or 4 (IL=1.44 mm; gear ratio≈20).

Evaluating the muscle-robot's performance

Measurements of the robotic system verified that muscle force is transferred to the robotic foot without significant mechanical artifacts. All moving parts in the system are small (moment of

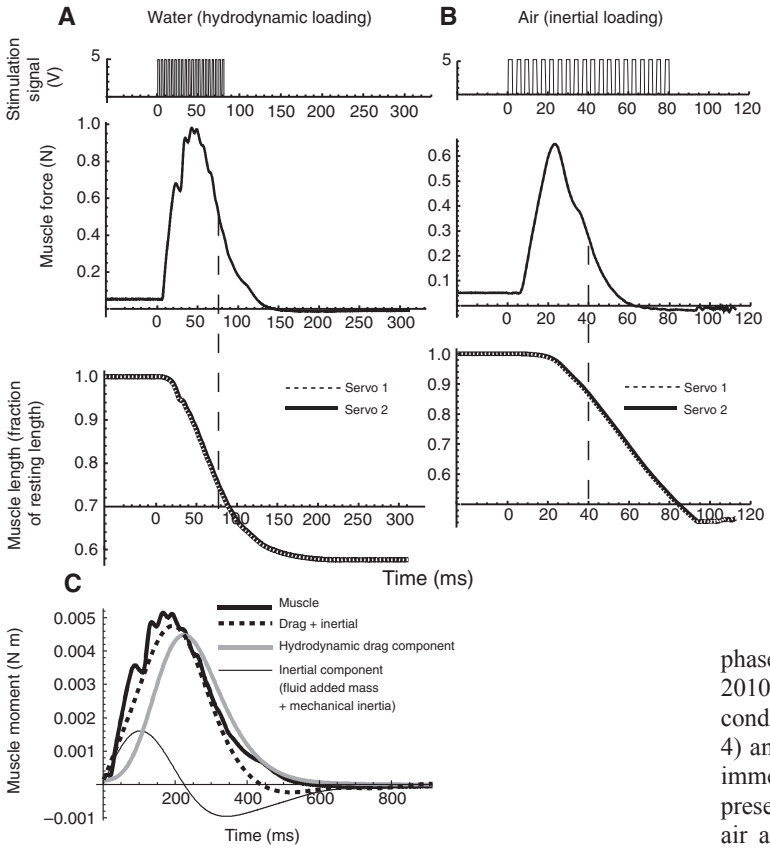

Fig. 2. Example raw data traces of electrical stimulation signal to the muscle, muscle force and shortening during (A) hydrodynamic loading and (B) inertial loading at gearing multiplier (GM)=1. The stimulation signal is the same for all experimental conditions. The vertical dashed lines represent the point at which muscle has produced 80% of total impulse (i.e. 80% of area under the force trace). Traces are unfiltered. (C) The muscle moment from A was decomposed into hydrodynamic drag and inertial force. Calculations are from modeling the frog foot as a flat plate (see Richards, 2008), where drag force=0.5×density×foot area×coefficient of drag×(distance to center of foot area×rotational foot velocity)^2 and inertial moment=(foot moment of inertia+rotational added mass)×foot angular acceleration.

inertia≈1×10^{-6} kg m^2) and friction and gravitational loads were negligible. In the absence of muscle, Servo 1 was manually pulled across its full range to verify that motion was correctly transferred to Servo 2 and the robotic foot (Fig. 1C). Except for a ~2 ms feedback delay (see below), the displacement signals were nearly identical, indicating negligible damping or elastic effects that would otherwise alter force transmission from Servo 1 to Servo 2 to the robotic foot. Additionally, Aurora motors have a hardware delay between force and displacement signals, resulting in a 2 ms lag of Servo 2 displacement behind Servo 1. This delay likely caused small force oscillations for water trials at low gear (Fig. 2A), but did not affect the other conditions (e.g. Fig. 2B). The servo control loop was simulated in Mathematica 7.0 (Wolfram Research, Champaign, IL, USA) to evaluate the bio-robot's performance with or without a 2 ms feedback delay. Simulations verified that a feedback delay causes force oscillations (similar to Fig. 2A); however, the overall force profile is not altered by the delay (data not shown). Therefore, the 2 ms delay was unlikely to influence the present findings.

For the present experiments, the effects of in-series tissue elasticity were not measured. Such effects can alter the timing of muscle velocity relative to the load. However, because the loads are very low in the present study, elastic stiffness of ~2500 N m^{-1} [estimated based on Roberts and Marsh (Roberts and Marsh, 2003)] would result in negligible elastic strain (~1–2%) under the muscle stresses observed here. Therefore, elastic effects unlikely confound the interpretation of the present results, but should be evaluated for future experiments if larger loads are tested.

Experimental design, data analysis and statistics

For all trials, only a single power stroke (shortening phase) was executed for each trial, simulating a single kick followed by a glide phase typical in 'burst-and-glide' swimming in frogs (Richards, 2010) rather than rhythmic cyclical contractions. Three experimental conditions were tested: loading (inertial *versus* fluid), GM (1, 2 and 4) and foot size (50, 100 and 150% length). The robotic foot was immersed either in water or air to explore muscle mechanics in the presence or absence of a hydrodynamic load. Throughout the study, air and water trials refer to inertial and hydrodynamic loading, respectively (air resistance is negligible). Although muscles are unlikely to face purely inertial loads during propulsion, understanding inertial effects are important because inertia may dominate during the retraction phase (e.g. swing phase during running, upstroke during flight or recovery stroke during swimming). Ground contact was not tested to avoid introducing gravitational loads that would confound the simple inertial versus hydrodynamic comparison. Six conditions were performed testing the effect of gearing and loading (i.e. GM=1, 2 and 4 each for fluid *versus* inertial loading). Three additional trials tested the effects of foot size at GM=1 in water. For each frog, each of the nine conditions were tested with nine separate muscle contractions (one trial per stimulation). To avoid effects of fatigue, isometric twitch contractions were performed periodically to verify that muscle remained within 10% of its initial force. Further, all conditions were randomized to eliminate effects of trial order. Following recording, data traces were analyzed between the onset time of muscle stimulation and the point when muscle force fell to 0.01 N. In some trials, the foot rotated the full range to hit the end of its travel before the muscle relaxed fully. In these cases, the data traces were truncated where the foot stopped. Prior to work and power calculations, a 20 Hz second-order forward–backward low-pass Butterworth filter was used for the muscle velocity traces. Net muscle work (time integral of instantaneous power) and power (work/contraction duration) were then computed.

To determine the effects of inertial *versus* hydrodynamic loading, mean differences in five muscle performance variables (peak stress, strain magnitude, mean shortening velocity, net work and net power) were evaluated with paired *t*-tests corrected by the sequential Bonferroni method (Quinn and Keough, 2002). All muscle performance variables were compared using a one-way ANOVA with the Tukey–Kramer HSD *post hoc* test to determine the effects of changing GM for either air or water trials. A two-way ANOVA

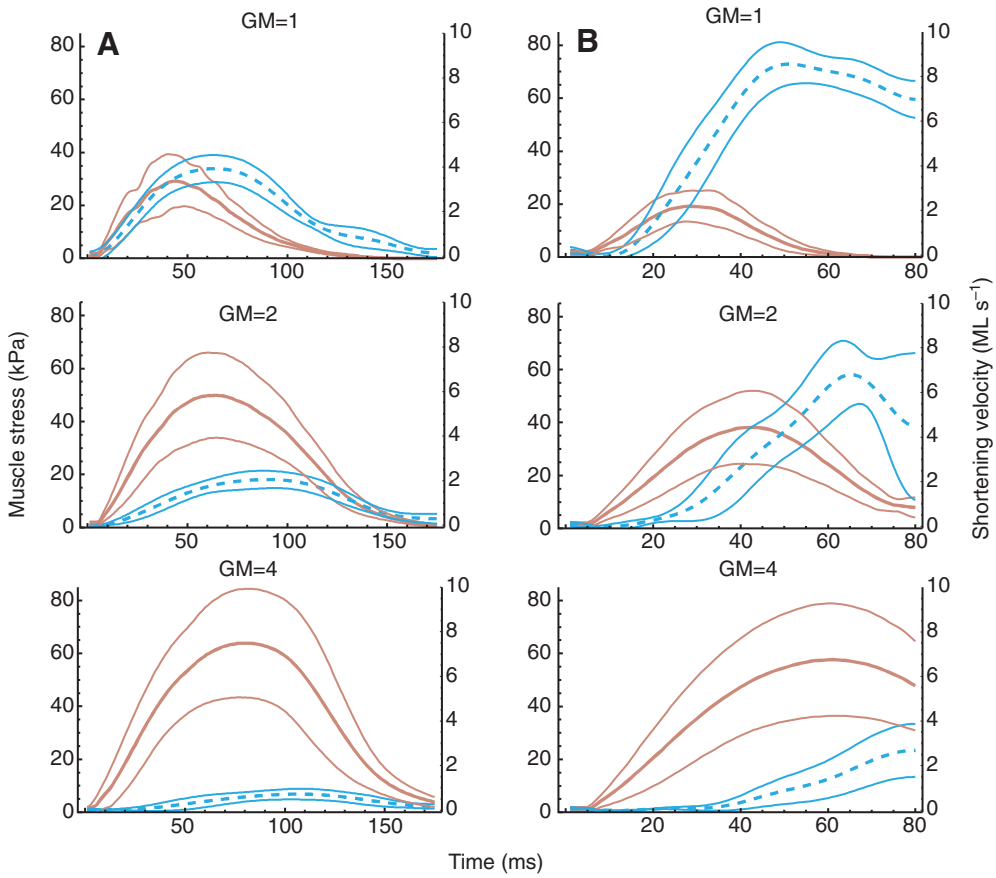

Fig. 3. Mean (thick) ±s.d. (thin) muscle stress (solid brown) and shortening velocity (dashed blue) traces averaged over *N*=6 animals for (A) water trials and (B) air trials. Upper, middle and lower panels show data for GM=1, 2 and 4, respectively, using the medium (100% length) foot size. ML, muscle length.

was used to test interacting effects of loading and gearing on the muscle performance parameters. Statistics were performed in SPSS 16.0 (SPSS Inc., Chicago, IL, USA).

RESULTS

Effects of loading environment (inertial *versus* fluid) of the robotic foot on muscle dynamics

Isolated muscle experiments yielded muscle stress, work and power outputs within the range observed from *in vivo* recordings from the PL during swimming (Richards and Biewener, 2007). During frog swimming, muscle force is due to the sum of inertial forces (limb inertia + fluid added mass; α acceleration) and fluid drag (proportional to velocity^2) (Gal and Blake, 1988). When the foot was immersed in water, the muscle produced force mainly in response to hydrodynamic drag, but also because of mechanical and hydrodynamic inertia (Fig. 2C). For most loading conditions tested, significant differences in contractile performance were observed between air and water trials (Fig. 3). At GM=2, for example, the muscle reached a significantly higher peak stress of 50.1±16.1 kPa in water trials *versus* 39.0±13.6 kPa in air (Fig. 4). Under hydrodynamic loading, the muscle reached maximum force as it approached peak shortening velocity (Fig. 3A), similar to F–L dynamics observed *in vivo* (Richards and Biewener, 2007). Despite higher force production in water, muscle work was similar between air and water trials, producing 5.30±2.12 and 6.67±2.93 J kg^{-1} muscle, respectively (P>0.05). In air, muscles shortened 0.26±0.02 muscle lengths (ML) at a mean velocity of 3.09±0.47 ML s^{-1} compared with 0.21±0.04 ML at 0.85±0.25 ML s^{-1} in water. Consequently, net power output of 63.57±27.20 W kg^{-1} muscle was significantly higher in air than 29.07±18.23 in water (ANOVA, P<0.05). The F–V phases [(peak force time–peak velocity time)/contraction duration] were strikingly different between air and water trials (Fig. 3). For intermediate gearing, the mean F–V phase was –0.08±0.04 for trials performed in water *versus* –0.33±0.03 for air trials (P<0.001, paired *t*-test).

Effects of gearing on muscle dynamics

Changing the GM influenced muscle performance in both air and water trials. For muscle contractions performed against fluid, increasing GM by twofold and fourfold significantly increased peak stress from 29.8±10.1 to 50.1±16.2 to 64.3±20.7 kPa (one-way ANOVA, P<0.05, N=6 frogs; Fig. 5A). Reciprocally, as GM increased, strain magnitude decreased significantly from 0.34±0.05 to 0.21±0.04 to 0.07±0.03 ML and mean shortening velocity decreased significantly from 1.76±0.35 to 0.85±0.25 to 0.31±0.12 ML s^{-1}. From GM=1 to GM=2, normalized work output increased slightly from 73.30±5.65 to 90.29±10.91% maximum, but decreased significantly to 41.04±19.19 at GM=4. Similarly, normalized power output did not differ significantly between 41.55±11.06 and 40.45±14.75% maximum at low and intermediate gearing, but decreased significantly to 19.63±9.02 at GM=4 (P<0.05). Similar to water trials, muscle stress increased significantly from 20.8±5.9 to 39.0±13.6 to 58.1±0.1 kPa as GM was increased from lowest to highest during air trials (Fig. 5B). Reciprocally, as GM increased, strain magnitude decreased significantly from 0.51±0.04 to 0.26±0.02 to 0.13±0.01 ML and mean shortening velocity decreased significantly from 4.85±0.74 to 3.09±0.47 to 1.25±0.29 ML s^{-1}. As GM increased from 1 to 2, normalized work and power output both increased significantly from 35.14±8.61 to 73.60±7.98% maximum and from 36.00±9.76 to 92.83±9.07% maximum, respectively. However,

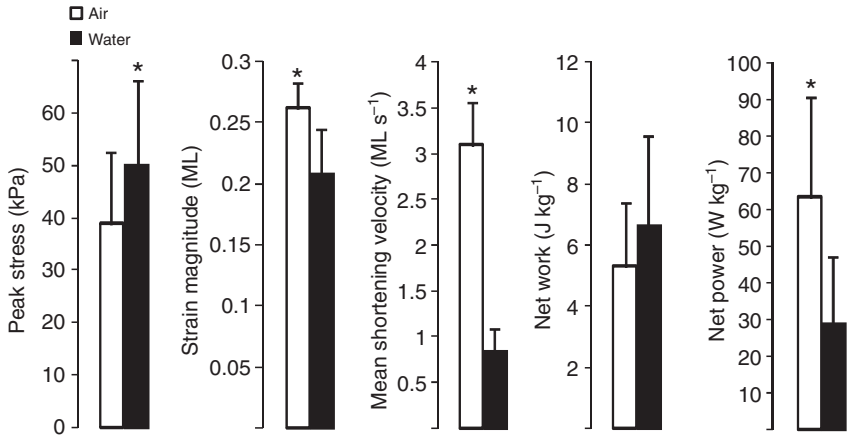

Fig. 4. Mean ± s.d. peak stress, strain magnitude, mean shortening velocity, net work and net power compared between air (white boxes) and water (black boxes) loading conditions. Only data from GM=2 and foot size=100% are shown. *Significant difference (P<0.05; Bonferroni-corrected paired t-tests).

there was no significant change in either normalized work or power as GM was increased to 4. Notably, the highest gearing caused the lowest work and power output in water trials, whereas the lowest gearing elicited the lowest work and power output in air trials.

Interacting effects of environment and gearing on muscle dynamics

Interactions between environment and gearing gave insight into muscle performance. Muscle F–L dynamics were highly sensitive to changes in either environment or gearing. Moreover, the effects of gearing on muscle power depended on inertial *versus* fluid loading, resulting in a significant environment–GM interaction (two-way ANOVA, P<0.001). Increasing GM from 1 to 2 in air trials caused a dramatic increase in normalized muscle power output followed by a decrease at GM=4 (Fig. 5B). However, the power increase due to the gearing change was not observed for the foot in water (Fig. 5A). Consequently, among all of the loading conditions, normalized power output was maximum at GM=2 during inertial loading.

Regardless of loading environment, mean muscle shortening velocity decreased as GM increased (Fig. 5). Similar to trends for power output, trials performed in water showed lower mean shortening velocities than trials performed in air. As GM increased, mean shortening velocity decreased from 1.76±0.35 to 0.85±0.25 to 0.311±0.12 ML s^{-1} during hydrodynamic loading *versus* 4.85±0.74 to 3.09±0.47 to 1.25±0.29 ML s^{-1} for inertial loading.

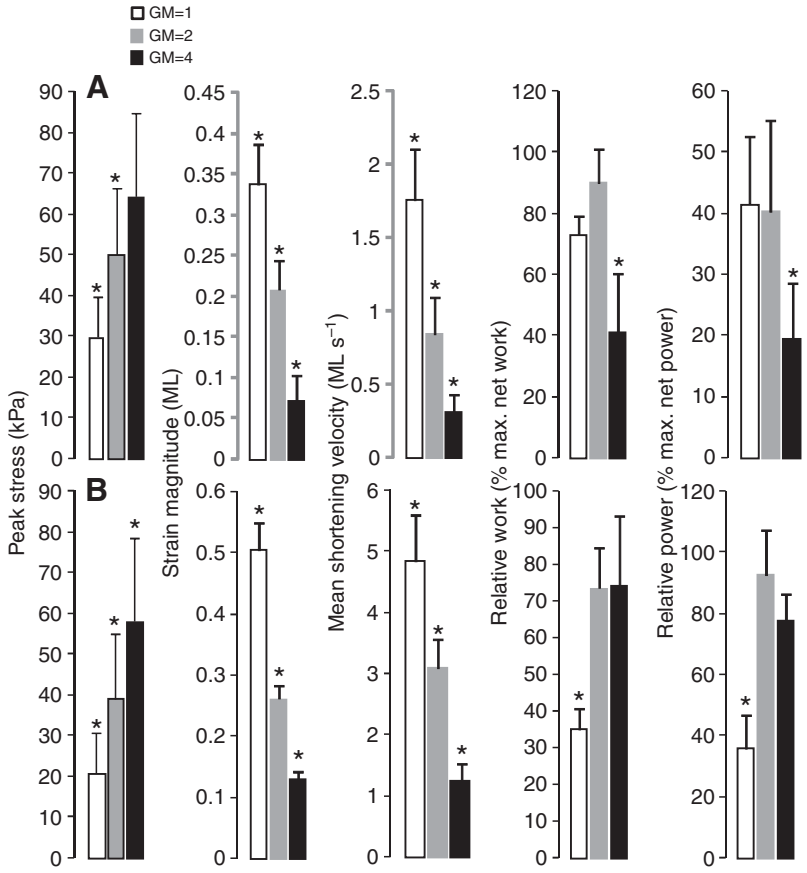

Fig. 5. The effect of gearing on muscle performance. Mean ± s.d. peak stress, strain magnitude, mean shortening velocity, relative work and relative power compared among GM=1 (white), 2 (grey) and 4 (black) using the medium (100% length) foot for (A) water and (B) air trials. *Significant difference (P<0.05; 1-way ANOVA with the Tukey–Kramer HSD *post-hoc* test).

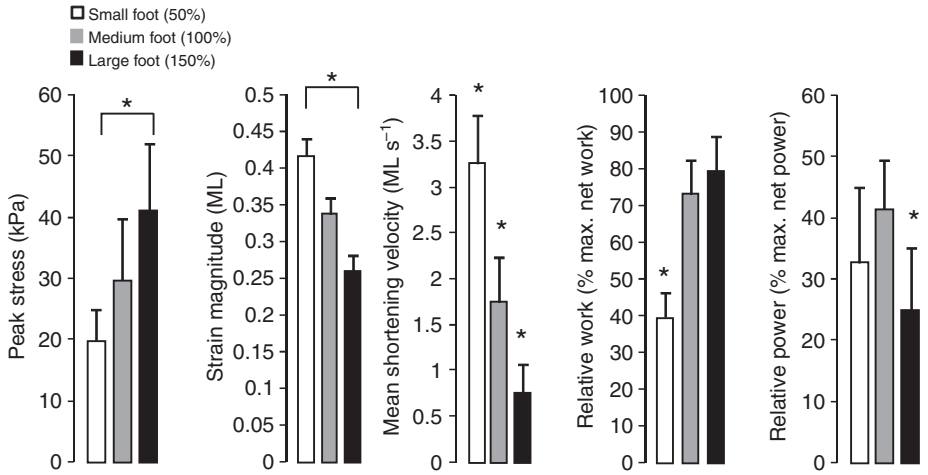

Fig. 6. The effect of foot size on muscle performance. Mean ± s.d. peak stress, strain magnitude, mean shortening velocity, relative work and relative power compared among small (50% length), medium (100%) and large (150%) foot sizes at GM=1 during hydrodynamic loading trials. *Significant difference (P<0.05; one-way ANOVA with the Tukey–Kramer HSD *post hoc* test).

Effects of foot size on muscle dynamics

In addition to changing the loading environment, muscle dynamics depended on the size of the robotic foot used (Fig. 6). For contractions in water at GM=1, peak stress increased slightly, but not significantly (ANOVA, P>0.05), from 19.9±5.2 to 29.8±10.1 to 41.2±11.0 kPa, differing significantly between the small and large foot sizes. Reciprocally, as foot size increased, mean shortening velocity decreased significantly from 3.26±0.29 to 1.76±0.35 to 0.76±0.17 ML s^{-1}. Normalized muscle work increased significantly from 39.7±12.7 to 73.9±5.6% maximum from the small to medium feet, but increased only slightly to 79.38±24.9% maximum for the largest foot. Additionally, as foot size increased, normalized power output increased slightly from 32.8±7.1 to 41.6±11.1% maximum, followed by a substantial decrease to 25.1±8.0% maximum for the largest foot.

DISCUSSION

Theory predicts that the dynamic aspects of muscle function (force and length changes) depend on the interactions between muscle and its environment (Daniel, 1995; Marsh, 1999; Aerts and Nauwelaerts, 2009). The goal of the present study was to experimentally measure muscle dynamics in response to physical loading conditions. Using a biologically inspired robotic frog foot driven by a *X. laevis* PL muscle, I explored muscle performance as a function of environment, gearing and foot size without changing the electrical stimulation to the muscle. Three hypotheses were tested, none of which are fully supported by the data. Firstly, I expected muscle force (and therefore power) to be higher with the foot in water rather than in air because of the considerably high drag and added mass of water (Gal and Blake, 1988) compared with the inertia of the limb. As expected, for a given gearing, peak muscle force was higher in water *versus* air. Despite increased force production in water, muscle work did not differ significantly between inertial and fluid loading for the present conditions tested. Furthermore, in air trials, the muscle shortened more rapidly and to shorter lengths for any given loading condition, generating higher power (Figs 4, 5). Secondly, increasing GM by shortening the muscle moment arm did not result in faster foot displacement (and therefore higher power) in both air and water. Regardless of loading, muscle work output increased from GM=1 to 2 (Fig. 5). Interestingly, power increased approximately twofold with the foot in air, yet decreased when the foot was submerged. Finally, smaller and larger foot sizes (compared with natural *X. laevis* foot size) each caused muscle power to decrease, rather than increase as expected. Interestingly, changes in both loading environment and gearing each caused dramatic (approximately twofold) shifts in muscle power output, whereas a ~10-fold increase in foot area influenced muscle power only modestly.

Intrinsic muscle F–V properties explain variation in muscle performance

F–V and power–velocity plots highlight the dramatic effects of gearing and environment on muscle performance. Diversity in loading conditions produced variation in muscle output, outlining an inverse relationship between peak force and muscle shortening velocity (Fig. 7A). The derived bell-shaped power–velocity curve suggests maximum power at ~2–4 ML s^{-1} (Fig. 7B), which is close to the range expected for *X. laevis* hindlimb muscle operating at maximum power (i.e. $0.3V_{max}$) (Lannergen, 1987). Although increasing GM from low to medium significantly decreased shortening velocity for all conditions, power increased for air trials yet decreased for water trials (Fig. 5). In air, the low inertial load of the mechanical parts caused the muscle to contract too rapidly for maximal power generation in the absence of hydrodynamic loading (Fig. 7C). When GM is doubled, the muscle shortened less for a given foot displacement, thus decreasing shortening velocity to (~0.2–$0.4V_{max}$) and increasing the muscle force and power available predicted by the F–V curve. Although doubling GM for water trials similarly elicited higher forces at lower speeds, the shortening velocity became too low (~0.1–$0.2V_{max}$) to generate substantial power. Increasing or decreasing foot size by more than twofold (fluid loading only) caused a slight decrease in power. Such small effects are surprising, suggesting that muscle performance against a fluid load is more sensitive to changes in gearing than to changes in propulsor area.

In addition to F–V properties that underlie main differences seen among loading conditions, other intrinsic muscle properties should also be considered. For example, inertia-loaded muscles shortened to ~50% of rest length at low gear *versus* ~13% at high gear, implying that F–L effects may be important. Yet muscles produced most of the force for a given trial (80% of total impulse) within the first ~10% of strain (Fig. 2B). Because the remaining 40% of shortening occured long after peak force, F–L effects are unlikely to influence muscle-load dynamics in this case. Interestingly for water at low gear, muscles produced most of the force after ~20% shortening *versus* ~13 and ~4% at middle and high gears. This suggests that F–L effects may reduce muscle power more strongly

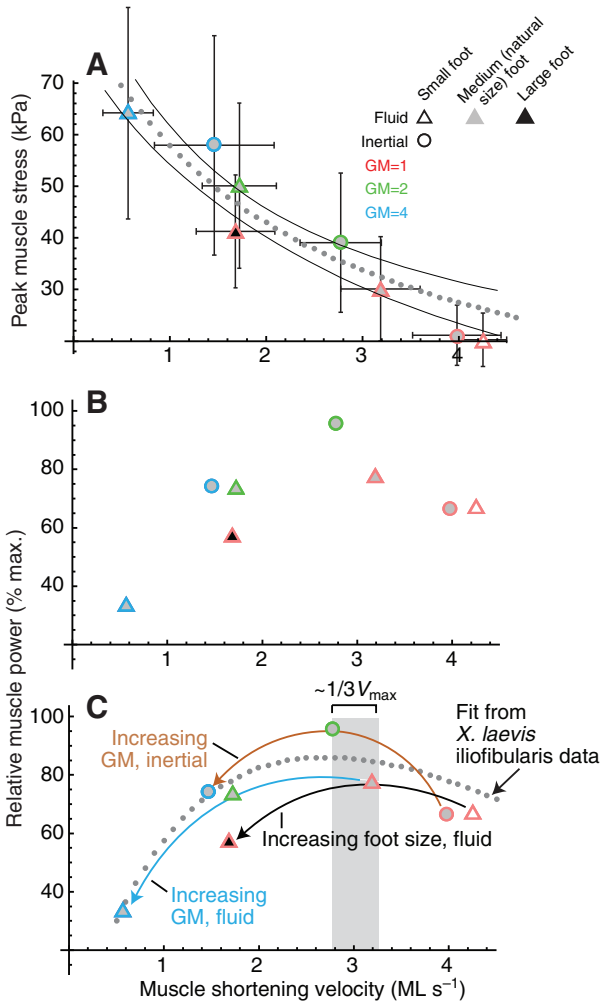

Fig. 7. (A) Peak muscle stress *versus* mean shortening velocity. (B) Relative muscle power *versus* mean shortening velocity. Relative muscle power was obtained by normalizing power values by the maximum power generated among all trials for a given frog. For all plots, circles are air trials and triangles are water trials at GM=1 (pink), 2 (green) and 4 (blue). White, grey and black indicate small (50%), medium (100%) and large (150%) foot sizes tested in water. (C) Power–velocity plot is repeated to suggest trends between air and water trials. The dotted line represents a fit for the above data based on *Xenopus laevis* iliofibularis muscle (Lannergen, 1987). For air trials, increasing GM from 1 to 2 lowers muscle shortening velocity to values close to 1/3V_{max} (based on *X. laevis* iliofibularis muscle) (Lannergen, 1987) where peak power is predicted. However, for water trials, increased GM lowers muscle velocity farther from 1/3V_{max}. Similar to air trials, increasing foot size causes power to increase by diminishing muscle velocity to ~1/3V_{max} at 100% size, followed by a decrease in power at 150% size. For this figure only, mean shortening velocity and net power were measured only within ±10% of peak force time. Error bars are ±s.d.

for water trials at low gear. Perhaps the above F–L effects in water explain why power was not significantly larger at GM=1 (*versus* GM=2), despite shortening near 1/3V_{max} (Fig. 7C). Future measurements of both F–V and F–L properties of *X. laevis* PL muscle will give further insight into the contractile behavior observed in the present setup.

Insight from present findings into *in vivo* muscle function

A central finding from the present study shows how muscle F–V timing differs between inertial and hydrodynamic loads, possibly giving insight into *in vivo* muscle function. Isolated muscle experiments from aquatic and terrestrial vertebrates established a general understanding that neural control can shift the timing of muscle activation with respect to length change (phase) to modulate contractile output (e.g. Altringham and Johnston, 1990; Ahn et al., 2003). *In vivo* studies on running birds reinforced this understanding, showing that changes in neural activation likely modulate work output by altering the relative timing of force and length change, producing F–V phases ±20% of stride duration (Daley et al., 2003; Gabaldón et al., 2004). Additionally, results presented here demonstrate that F–V timing shifts emerge not only from neural control, but also from changes in loading. In water, drag (proportional to foot or muscle velocity^2) dominates over inertia (Fig. 2C), causing phase coupling between muscle force and velocity (Fig. 3). Similarly, during *X. laevis* swimming, *in vivo* muscle F–V phase does not change significantly (±~3% of contraction duration), despite substantial variation in the relative timing of neural activation and shortening (C.T.R., unpublished observations). In contrast, without fluid loading, the muscle in the present setup is loaded by the limb's inertia. Consequently, force develops before muscle velocity, peaking at maximum muscle acceleration (Fig. 3). Analogously, in mallards, peak lateral gastrocnemius force occurs far before peak shortening velocity (large F–V phase) during walking, but peaks near maximum velocity during swimming (small F–V phase) (Biewener and Corning, 2001). Because the muscle activation phase was similar for swimming and walking, contractile differences found in mallards may emerge largely from the loading shift between gravitational and inertial loading *versus* hydrodynamic loading, rather than neural control. In light of prior *in vivo* studies, data from the present study predict that drag-based swimmers cannot modulate F–V timing by neural timing alone, as observed in terrestrial locomotion. Rather, *in vivo* F–V phase shifts perhaps occur as the relative magnitudes of inertia (fluid added mass and limb inertia) and drag change, depending on the dynamic orientation, shape and size of the fins or feet. Future experiments using the present setup can test these predictions.

Limitations of the robotic setup

The robotic setup lacks certain components that will enhance the understanding of muscle dynamics in swimming. A translating stage to be used in subsequent studies (Fig. 1A) will simulate both forward swimming of the body and extension of limb joints to mimic swimmers such as frogs (Gal and Blake, 1988), waterfowl (Johansson and Lindhe Norberg, 2001), turtles (Pace et al., 2001) or mammals (Gillis and Blob, 2001). Further modifications of the robotic setup will include dynamic aspects of morphology. Gear ratio was defined using both a constant IL and OL; however, both lengths can change dynamically. For instance, limb posture and/or orientation of the reaction force may increase the gear ratio by increasing OL throughout a stride (Biewener, 1989; Carrier et al., 1998; Roberts and Scales, 2004). Alternatively, within a shortening muscle, fiber angles can rotate with respect to the muscle's load axis, dynamically changing the ratio of fiber shortening to whole-muscle shortening (Azizi et al., 2008), altering the speed of muscle fiber shortening with respect to the speed of the load. Dynamic gear shifts (e.g. Roberts and Marsh, 2003) could be implemented using the present approach. Additionally, non-rigid fins could be incorporated into the present setup (see Lauder et al., 2006; Tangorra et al., 2007) to generate more biologically realistic flow patterns around the robotic foot. Lastly, an antagonist muscle could be added to re-lengthen the PL [see novel work by Farahat and Herr (Farahat and Herr, 2006; Farahat and Herr, 2010)] to better emulate the burst-and-glide behavior that is common in swimmers.

From a neural control perspective, the above modifications will enable experiments that map the relationship between stimulation input and muscle mechanical output. Work loop literature shows that input parameters can be 'tuned' to modify muscle work or power depending on strain frequency and magnitude (e.g. Josephson and Stokes, 1989; Full et al., 1998) or strain trajectory (Askew and Marsh, 1997; Ellerby and Askew, 2007). Likewise, muscle-robotic experiments could test how different foot or fin morphologies affect the tuning of activation parameters. Hence, the modified setup will further the understanding of how mechanical environment and neural control interact to modulate muscle output.

CONCLUSIONS

I propose the use of the muscle-robotic setup as a powerful, but simple tool for physiologists to explore muscle function under realistic dynamic loading. I demonstrate that varying the mechanical environment of isolated muscle elicits a broad range of contractile output, independently of neural control. Specifically, muscles dominated by inertial loading produce force that is out of phase with velocity, whereas drag-based loading causes force and velocity to coincide. This suggests that peak force during hydrodynamic loading may be more severely limited by the muscle's F–V relationship than force produced during inertial loading. Additionally, findings also suggest how modifications in limb morphology either increase or decrease muscle power depending on the loading regime as well as the absolute gear ratio of the joint. Further, altering the foot size diminishes muscle power only modestly, suggesting that contractile output is considerably more sensitive to changes in gearing than to foot area when operating against a fluid dynamic load.

ACKNOWLEDGEMENTS

I thank Chris Stokes for his wealth of electronics knowledge and for help with the FPGA controller. Donald Rogers helped with machining. I also am very grateful to Andrew Biewener for lending me equipment and lab space for preliminary experiments before my present lab was operating. I thank Christofer Clemente and Monica Daley both for critical comments during manuscript preparation and for helpful discussions on muscle mechanics. I also thank Anna Ahn for providing the suction electrode and for extremely detailed and insightful comments on my manuscript. I thank all reviewers for fair and thoughtful comments. This work was entirely funded by the Rowland Junior Fellows Program.

REFERENCES

Aerts, P. and Nauwelaerts, S. (2009). Environmentally induced mechanical feedback in locomotion: frog performance as a model. *J. Theor. Biol.* **261**, 372-378.

Ahn, A. N., Monti, R. J. and Biewener, A. A. (2003). *In vivo* and *in vitro* heterogeneity of segment length changes in the semimembranosus muscle of the toad. *J. Physiol.* **549**, 877-888.

Altringham, J. D. and Johnston, I. A. (1990). Modeling muscle power output in a swimming fish. *J. Exp. Biol.* **148**, 395-402.

Askew, G. and Marsh, R. (1997). The effects of length trajectory on the mechanical power output of mouse skeletal muscles. *J. Exp. Biol.* **200**, 3119-3131.

Azizi, E., Brainerd, E. L. and Roberts, T. J. (2008). Variable gearing in pennate muscles. *Proc. Natl. Acad. Sci.* **105**, 1745-1750.

Biewener, A. A. (1989). Scaling body support in mammals: limb posture and muscle mechanics. *Science* **245**, 45-48.

Biewener, A. A. and Corning, W. R. (2001). Dynamics of mallard (*Anas platyrhynchos*) gastrocnemius function during swimming versus terrestrial locomotion. *J. Exp. Biol.* **204**, 1745-1756.

Bowtell, G. and Williams, T. L. (1991). Anguilliform body dynamics: modelling the interaction between muscle activation and body curvature. *Philos. Trans. Biol. Sci.* **334**, 385-390.

Carrier, D., Gregersen, C. and Silverton, N. (1998). Dynamic gearing in running dogs. *J. Exp. Biol.* **201**, 3185-3195.

Daley, M. A. and Biewener, A. A. (2003). Muscle force-length dynamics during level versus incline locomotion: a comparison of *in vivo* performance of two guinea fowl ankle extensors. *J. Exp. Biol.* **206**, 2941-2958.

Daley, M. A., Voloshina, A. and Biewener, A. A. (2009). The role of intrinsic muscle mechanics in the neuromuscular control of stable running in the guinea fowl. *J. Physiol.* **587**, 2693-2707.

Daniel, T. L. (1995). Invertebrate swimming: integrating internal and external mechanics. *Symp. Soc. Exp. Biol.* **49**, 61-89.

Daniel, T. L. and Meyhofer, E. (1989). Size limits in escape locomotion of carridean shrimp. *J. Exp. Biol.* **143**, 245-265.

Dial, K. P., Kaplan, S. R., Goslow, G. E., Jr and Jenkins, F. A., Jr (1987). Structure and neural control of the pectoralis in pigeons: implications for flight mechanics. *Anat. Rec.* **218**, 284-287.

Ekeberg, Ö. (1993). A combined neuronal and mechanical model of fish swimming. *Biol. Cybern.* **69**, 363-374.

Ellerby, D. J. and Askew, G. N. (2007). Modulation of flight muscle power output in budgerigars *Melopsittacus undulatus* and zebra finches *Taeniopygia guttata*: *in vitro* muscle performance. *J. Exp. Biol.* **210**, 3780-3788.

Farahat, W. and Herr, H. (2006). Workloop energetics of antagonist muscles. *Conf. Proc. IEEE Eng. Med. Biol. Soc.* **1**, 3640-3643.

Farahat, W. and Herr, H. (2010). Optimal workloop energetics of muscle-actuated systems: an impedance matching view. *PLoS Comput. Biol.* **6**, e1000795.

Freadman, M. (1979). Role partitioning of swimming musculature of striped bass, *Morone saxatilis* Walbaum, and bluefish, *Pomatomus saltatrix* L. *J. Fish Biol.* **15**, 417-423.

Full, R. J., Stokes, D. R., Ahn, A. N. and Josephson, R. K. (1998). Energy absorption during running by leg muscles in a cockroach. *J. Exp. Biol.* **201**, 997-1012.

Gabaldón, A. M., Nelson, F. E. and Roberts, T. J. (2004). Mechanical function of two ankle extensors in wild turkeys: shifts from energy production to energy absorption during incline versus decline running. *J. Exp. Biol.* **207**, 2277-2288.

Gal, J. M. and Blake, R. W. (1988). Biomechanics of frog swimming: II. Mechanics of the limb-beat cycle in *Hymenochirus Boettgeri*. *J. Exp. Biol.* **138**, 413-429.

Gillis, G. (2000). Patterns of white muscle activity during terrestrial locomotion in the American eel (*Anguilla rostrata*). *J. Exp. Biol.* **203**, 471-480.

Gillis, G. B. and Blob, R. W. (2001). How muscles accommodate movement in different physical environments: aquatic vs. terrestrial locomotion in vertebrates. *Comp. Biochem. Physiol.* **131A**, 61-75.

Gordon, A. M., Huxley, A. F. and Julian, F. J. (1966). The variation in isometric tension with sarcomere length in vertebrate muscle fibres. *J. Physiol.* **184**, 170-192.

Hedrick, T. L., Tobalske, B. W. and Biewener, A. A. (2003). How cockatiels (*Nymphicus hollandicus*) modulate pectoralis power output across flight speeds. *J. Exp. Biol.* **206**, 1363-1378.

Hill, A. V. (1938). The heat of shortening and the dynamic constants of muscle. *Proc. R. Soc. Lond. B* **126**, 136-195.

Ijspeert, A., Crespi, A. and Cabelguen, J.-M. (2005). Simulation and robotics studies of salamander locomotion. *Neuroinformatics* **3**, 171-195.

Ijspeert, A. J., Crespi, A., Ryczko, D. and Cabelguen, J.-M. (2007). From swimming to walking with a salamander robot driven by a spinal cord model. *Science* **315**, 1416-1420.

Johansson, L. and Lindhe Norberg, U. (2001). Lift-based paddling in diving grebe. *J. Exp. Biol.* **204**, 1687-1696.

Josephson, R. (1985). The mechanical power output from striated muscle during cyclic contraction. *J. Exp. Biol.* **114**, 493-512.

Josephson, R. (1999). Dissecting muscle power output. *J. Exp. Biol.* **202**, 3369-3375.

Josephson, R. K. and Stokes, D. R. (1989). Strain, muscle length and work output in a crab muscle. *J. Exp. Biol.* **145**, 45-61.

Lannergren, J. (1987). Contractile properties and myosin isoenzymes of various kinds of *Xenopus* twitch muscle fibers. *J. Muscle Res. Cell Motil.* **8**, 260-273.

Lauder, G. V., Madden, P. G. A., Mittal, R., Dong, H. and Bozkurttas, M. (2006). Locomotion with flexible propulsors: I. Experimental analysis of pectoral fin swimming in sunfish. *Bioinspir. Biomim.* **1**, s25-s34.

Machin, K. E. and Pringle, J. W. S. (1960). The physiology of insect fibrillar muscle. III. The effect of sinusoidal changes of length on a beetle flight muscle. *Proc. R. Soc. Lond. B* **152**, 311-330.

Mann, R. A. and Hagy, J. (1980). Biomechanics of walking, running, and sprinting. *Am. J. Sports Med.* **8**, 345-350.

Marsh, R. (1999). How muscles deal with real-world loads: the influence of length trajectory on muscle performance. *J. Exp. Biol.* **202**, 3377-3385.

Pace, C. M., Blob, R. W. and Westneat, M. W. (2001). Comparative kinematics of the forelimb during swimming in red-eared slider (*Trachemys scripta*) and spiny softshell (*Apalone spinifera*) turtles. *J. Exp. Biol.* **204**, 3261-3271.

Quinn, G. P. and Keough, M. J. (2002). *Experimental Design and Data Analysis for Biologists*. Cambridge: Cambridge University Press.

Richards, C. T. (2008). The kinematic determinants of anuran swimming performance: an inverse and forward dynamics approach. *J. Exp. Biol.* **211**, 3181-3194.

Richards, C. T. (2010). Kinematics and hydrodynamics analysis of swimming anurans reveals striking inter-specific differences in the mechanism for producing thrust. *J. Exp. Biol.* **213**, 621-634.

Richards, C. T. and Biewener, A. A. (2007). Modulation of *in vivo* muscle power output during swimming in the African clawed frog (*Xenopus laevis*). *J. Exp. Biol.* **210**, 3147-3159.

Roberts, T. J. and Marsh, R. L. (2003). Probing the limits to muscle-powered accelerations: lessons from jumping bullfrogs. *J. Exp. Biol.* **206**, 2567-2580.

Roberts, T. J. and Scales, J. A. (2004). Adjusting muscle function to demand: joint work during acceleration in wild turkeys. *J. Exp. Biol.* **207**, 4165-4174.

Roberts, T. J., Marsh, R. L., Weyand, P. G. and Taylor, C. R. (1997). Muscular force in running turkeys: the economy of minimizing work. *Science* **275**, 1113-1115.

Rome, L. C., Loughna, P. T. and Goldspink, G. (1984). Muscle fiber activity in carp as a function of swimming speed and muscle temperature. *Am. J. Physiol. Regul. Integr. Comp. Physiol.* **247**, R272-R279.

Tangorra, J., Davidson, S. N., Hunter, I. W., Madden, P. G. A., Lauder, G. V., Dong, H., Bozkurttas, M. and Mittal, R. (2007). The development of a biologically inspired propulsor for unmanned underwater vehicles. *IEEE J. Ocean. Eng.* **32**, 533-550.

Tanji, J. and Kato, M. (1973). Firing rate of individual motor units in voluntary contraction of abductor digiti minimi muscle in man. *Exp. Neurol.* **40**, 771-783.

Tytell, E. D., Hsu, C.-Y., Williams, T. L., Cohen, A. H. and Fauci, L. J. (2010). Interactions between internal forces, body stiffness, and fluid environment in a neuromechanical model of lamprey swimming. *Proc. Natl. Acad. Sci.* **107**, 19832-19837.